RSC Advances

PAPER

View Article Online
View Journal | View Issue

Cite this: *RSC Adv.*, 2018, **8**, 38631

Ultrafine MnO_2 nanowires grown on RGO-coated carbon cloth as a binder-free and flexible supercapacitor electrode with high performance

Zhihui Xu,[a] Shishuai Sun,*[a] Wen Cui,[b] Dan Yu[a] and Jiachun Deng*[a]

Received 10th July 2018
Accepted 7th November 2018

DOI: 10.1039/c8ra05890c

rsc.li/rsc-advances

Reduced graphene oxide coated carbon cloth has been used as a substrate for the growth of ultrafine MnO_2 nanowires (CC/RGO/MnO_2), forming binder-free and flexible supercapacitor electrode materials. The experimental results indicate that a maximum area-specific capacitance of 506.8 mF cm^{-2} was gained from the CC/RGO/MnO_2 electrode at the current density of 0.128 mA cm^{-2}. Furthermore, the electrode exhibits excellent cycling stability (98.6% specific capacitance was still retained after 10 000 galvanostatic charge–discharge (GCD) tests when the current density was 1.28 mA cm^{-2}). What's more, the area-specific capacitance of the CC/RGO/MnO_2 electrode was hardly changed, when the electrode was operated under bending mechanical conditions. In addition, the charge storage performance and mechanism of the MnO_2 nanostructures was discussed.

1. Introduction

Supercapacitors (SCs) as a new type of green pollution-free energy storage device have attracted significant research attention in recent years owing to their unique properties such as fast charge–discharge ability, high power density, excellent reversibility and good cycling performance.[1–3] Flexible, light-weight and wearable supercapacitors have attracted great interest in energy storage due to their potential applications in portable electronic devices, flexible displays and mobile phones.[4–7] To promote these advanced supercapacitors for more practical applications in energy storage devices, great efforts have been directed toward the design and synthesis of high specific electrochemical capacitance and flexible electrode materials.[8–10]

Among all kinds of electrode materials, MnO_2 has been widely studied as the electrode material with most potential for supercapacitors due to its large theoretical specific capacitance (1370 F g^{-1}), low cost and natural abundance, and it has been studied deeply.[11–14] However, the development of MnO_2 based electrode materials is affected by the internal defects, including low conductivity, slow ion transport, and large volume changes during charging and discharging, which make it difficult to obtain high specific capacity, high rate capability and good cyclic stability.[15–18] Therefore, in order to overcome these shortcomings, researchers are trying to develop new morphology and structure to increase their specific surface area.[19–21]

So far there is a vast literature of supercapacitive MnO_2 in which capacitance values close to the theoretical quantity of 1370 F g^{-1} have been reported.[11,16,22] However, most of these studies utilized a rather thin MnO_2 film with mass loadings less than 0.5 mg cm^{-2}. Therefore, the total capacitance (in unit of F) and amount of charges (in unit of C) are small, which will not meet certain applications that require high area or volumetric capacitance. As a new type of two-dimensional nano-carbon material, graphene has the advantages of high specific surface area (theoretical specific surface area exceeding 2600 m^2 g^{-1}), good electrical conductivity and mechanical properties, which cannot be replaced by other energy storage electrode materials. Previously reports show that the graphene can increase the specific surface area of the substrate, so that to increase the loading of the active material on the substrate and its area-specific capacity.[16]

In this work, we chose carbon cloth (CC) with good flexibility as substrate for the growth of MnO_2 materials due to its high conductivity and 3D open porous structure, which can provide more channels for ion transmission and enhance electrical conductivity.[23,24] In addition, the reduced graphene oxide (RGO) was coated on the surface of carbon cloth (CC/RGO) in order to further enhance the mass loading of MnO_2.[25–27] Subsequently, the nanowires of MnO_2 were synthesized by hydrothermal method to growth on the surface of CC/RGO (CC/RGO/MnO_2). The hybrid electrode shows a excellent electrochemical performance, such as high specific capacitance, excellent rate capability, superior cycling stability and mechanical reliability due to its high-electron/ion-transfer rate, large electrolyte infiltrate area, and more electroactive reaction sites.

[a]*College of Science, Tianjin University of Technology, Tianjin 300384, China. E-mail: sssdashuai@163.com; dengjiachun@tjut.edu.cn*

[b]*College of Physics and Materials Science, Tianjin Normal University, Tianjin, 300387, China*

2. Experimental section

All reagents in the experiments are of analytical grade and used without further purification. All the solutions were prepared in deionized water.

2.1. Synthesis of CC/RGO

The CC (purchased from Taiwan carbon energy company and surface density: 12.5 mg cm^{-2}, thickness: 0.36 mm) with the size of 1 cm × 3 cm was first pretreated successively with hydrochloric acid (6 M), acetone, deionized water and ethanol by ultrasonic cleaning, and dried at 60 °C overnight. The mass of carbon cloth was denoted as M_1. GO was purchased from Nanjing Xianfeng nanophase materials Science and Technology Ltd. The CC was immersed into the GO suspension (1 mg mL^{-1}) for 1 h to ensure GO coated on the CC surface and dried. Then it was placed in the HI solution for 1 h at room temperature in order to reduce the GO.[28] Finally, the sample was washed with deionized water by ultrasonication and vacuum dried at 60 °C for the night.

2.2. Synthesis of CC/RGO/MnO_2

The composite of MnO_2 nanowires immobilized on the CC/RGO was synthesized by a facile hydrothermal method. In a typical synthesis process, the above formed CC/RGO composite was immersed into 40 mL solution with a concentration of 0.12 M $KMnO_4$. The CC/RGO and solution were then transferred into a 50 mL Teflon-lined stainless steel autoclave. The autoclave was sealed and hydrothermally treated at 180 °C for 900 min, after cooling to room temperature. The product was washed several times with deionized water and ethanol, and then dried at 60 °C overnight. Ultimately the CC/RGO/MnO_2 electrode was obtained. The quality of obtained CC/RGO/MnO_2 electrode was denoted as M_2. The mass of the active material on each square centimeter of CC was calculated by $(M_2 - M_1)/3 = 1.28$ mg cm^{-2}.

2.3. Materials characterization

Field-emission scanning electron microscopy (SEM, Quanta FEG 250 operated at 8 kV), transmission electron microscopy (TEM) and high-resolution TEM (HRTEM) were used to observe the morphology and microstructure of the CC/RGO/MnO_2 materials. Crystal structures of as-fabricated samples were characterized by X-ray diffraction system (XRD, Rigaku, D/MAX-2500, Japan) with Cu-Kα_1 radiation ($\lambda = 1.54056$ Å) and HRTEM. X-ray photoelectron spectroscopy (XPS, ESCALAB 250Xi) was employed to confirm the compositions and electronic properties.

2.4. Electrochemical performance measurements

Electrochemical performances were carried out on an electrochemical workstation (PGSTAT 302N) in a three-electrode configuration mode consisting of a CC/RGO/MnO_2 (1 cm × 1 cm) electrode as working electrode, a platinum foil (1 cm × 1 cm) as the counter electrode and a silver/silver chloride (Ag/AgCl) as reference electrode in 1 M Na_2SO_4 electrolyte. Cyclic voltammogram (CV) curves were measured under different scan rates of 5, 10, 20, 50 and 100 mV s^{-1} in the potential window of 0–0.8 V (*vs.* Ag/AgCl). GCD tests were done at different current densities of 0.128, 0.256, 0.64, 1.28 and 2.56 mA cm^{-2} over the potential range of 0–0.8 V (*vs.* Ag/AgCl), and electrochemical impedance spectroscopy (EIS) test was also performed using a frequency range of 0.1 Hz–100 kHz at open circuit voltage with the amplitude of 5 mV. The electrochemical cyclic stability of the CC/RGO/MnO_2 electrode was studied by repeating the GCD measurement at the current density of 1.28 mA cm^{-2} for 10 000 cycles. The specific areal capacitance was calculated using the equation:[29]

$$C = I\Delta t/(\Delta V S) \quad (1)$$

where C is the specific areal capacitance (mF cm^{-2}) and I, Δt, ΔV, and S are the discharge current (A), the discharge time (s) take in the potential range, the discharge potential range (V), and active materials area of the electrode (cm^2), respectively.

3. Results and discussion

The schematic illustration of the typical experiment process is shown in Fig. 1. In this study, 3D flexible lightweight of the CC were immersed in the GO suspension, and then GO was reduced by hydroiodic acid (HI). The CC/RGO was applied both as reducing agents and scaffolds for the MnO_2 growth. Subsequently, the MnO_2 nanostructures with controlled morphologies grew on the surface of the CC/RGO based on the self-limiting reaction between carbon and $KMnO_4$ in neutral aqueous solution through the hydrothermal method.[30] The reaction can be expressed as follows:[31,32]

$$4MnO_4^- + 3C + H_2O \rightarrow 4MnO_2 + CO_3^{2-} + 2HCO_3^- \quad (2)$$

Fig. 2a shows the interconnected 3D scaffold structure of the CC template, providing a higher porosity and surface area than the traditional graphene film. Fig. 2b and c show the typical SEM images of the CC/RGO at low and high magnification. The graphene sheets in the CC are directly contact with each other without obvious breaks. Fig. 2d–f shows the SEM images of the CC/RGO/MnO_2 at different magnifications. The results show that the morphology of the CC/RGO surface was covered completely with the 1D ultrafine MnO_2 nanowires, which forms a 3D open porous structure, providing sufficient space for the change of the volume of the active material during charging and discharging. This special structure not only promotes the transport of electrons for rapid redox reactions, but also improves the contact area of the electrode/electrolyte to accelerate the charge storage reaction.

In the present work, the ultrafine MnO_2 nanowires grown on the CC/RGO can be obtained simply *via* a modified hydrothermal method. The morphology of the MnO_2 was studied by TEM observation. It can be seen from Fig. 3a and b, many uniform MnO_2 nanowires were synthesized, and the size of the MnO_2 nanowires were ~5 nm in diameter. Fig. 3c displays

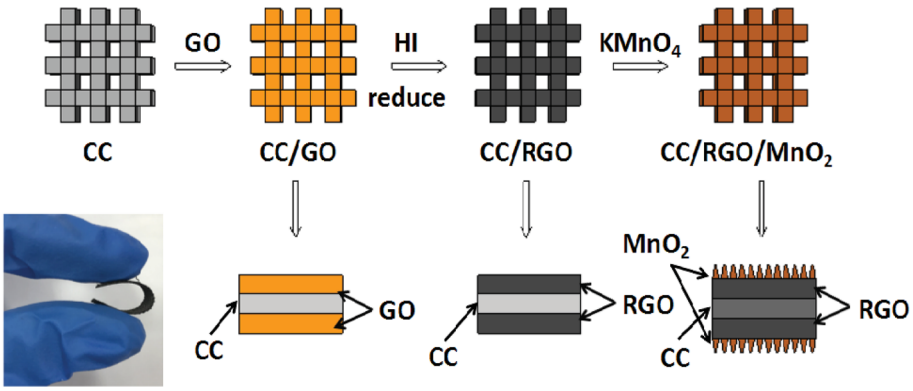

Fig. 1 Schematic diagram of the fabrication of the CC/RGO/MnO_2.

HRTEM images of the MnO_2 nanowires. This HRTEM image indicated that the nature of the MnO_2 nanowires were single crystals. Additionally, according to the HRTEM image in the inset of Fig. 3c, the interplanar spacing between the adjacent lattice planes was approximately 0.31 nm, corresponding to the (310) crystal plane of α-MnO_2.

In order to further confirm the component of the CC/RGO/MnO_2 composite material, the XRD pattern of the composites was obtained, as shown in Fig. 3d. In this figure, two strong peaks marked with "#" were originated from the CC (substrate) and RGO, and other peaks can be indexed to the MnO_2. The diffraction peak of the composite was completely consistent with the diffraction data of the standard card (JCPDS: 44-0141),[15] which was in accordance with the results of TEM. Due to the presence of the CC in the composite material, the carbon cloth had better crystallinity and a stronger peak. Therefore, the

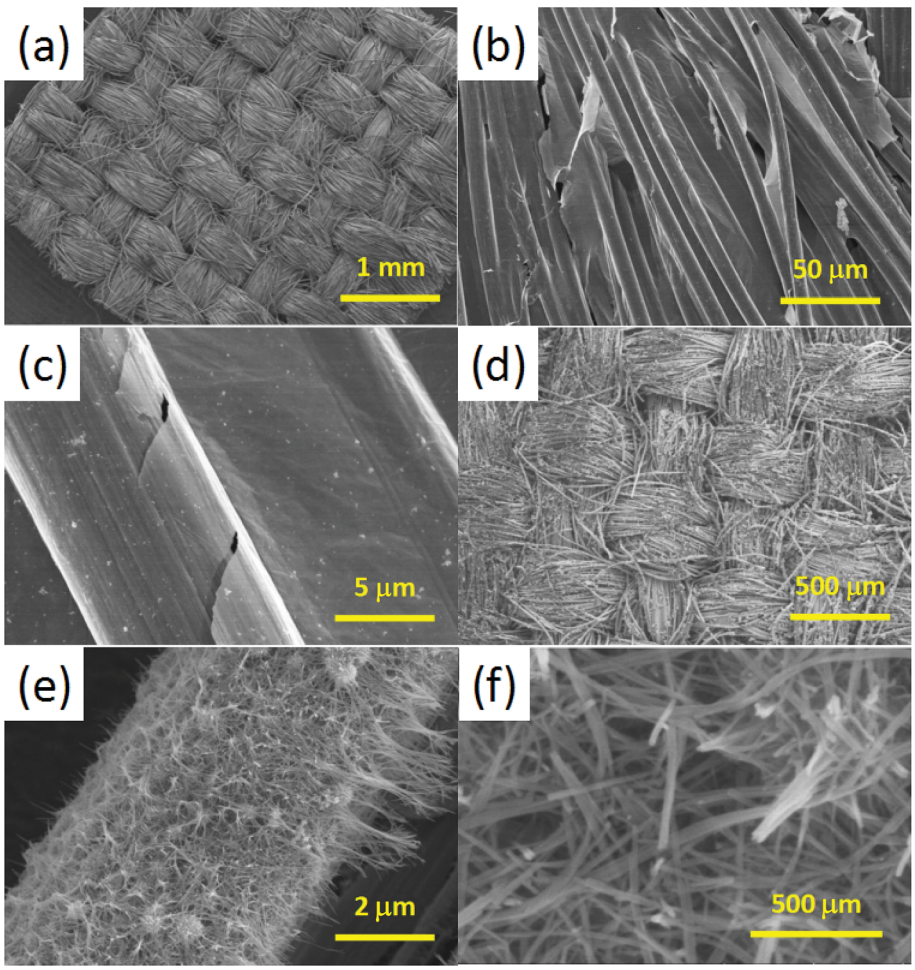

Fig. 2 (a) SEM images of the CC at low magnification. (b) and (c) SEM images of the CC/RGO at low and high magnification. (d–f) SEM images of the CC/RGO/MnO_2 with different magnification.

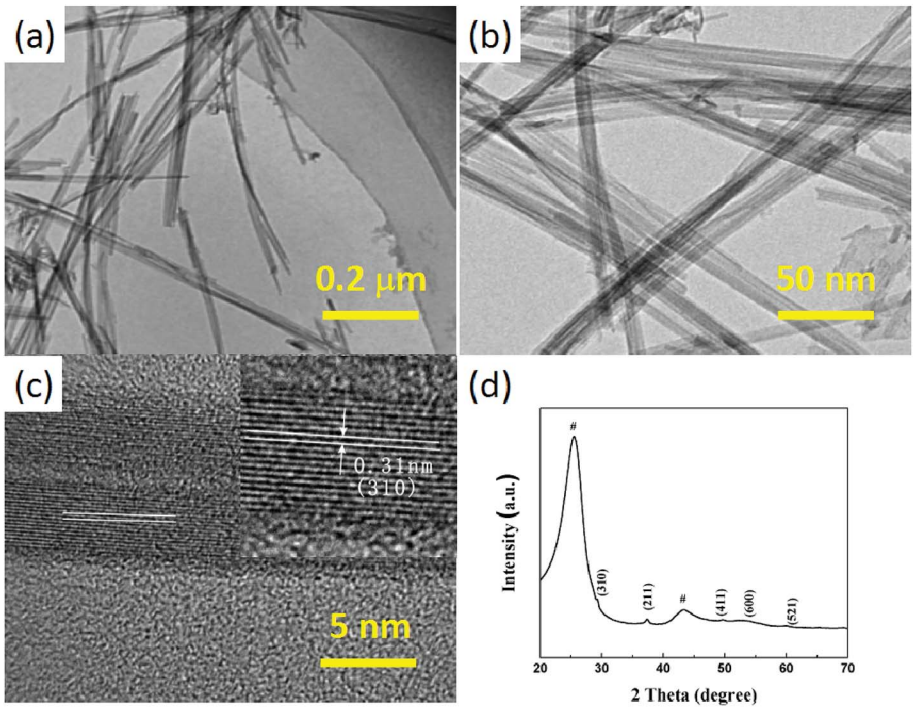

Fig. 3 (a) Low and (b) high magnifications TEM images of the MnO_2 nanowires. (c) HRTEM image of the MnO_2 nanowires. (d) XRD pattern of the CC/RGO/MnO_2.

peak of MnO_2 in the CC/RGO/MnO_2 composites was annihilated, leading to the weaker peak of the MnO_2. Moreover, no other crystalline impurities were detected in the prepared product.

In order to further determine the chemical components in the CC/RGO/MnO_2, the XPS analysis was performed. Fig. 4a shows the XPS spectra of the CC/RGO/MnO_2. The core levels of C, O, and Mn in the XPS full spectrum of the CC/RGO/MnO_2 hybrid confirmed the desired chemical composition. Fig. 4b presented the core-level Mn $2p^{3/2}$ and Mn $2p^{1/2}$ peaks having binding energies (BEs) at 642.1 and 653.9 eV, respectively, with a spin-energy separation of 11.8 eV, which were matched with a +4 formal oxidation state for the Mn atoms.[33] In the O 1s XPS spectrum (Fig. 4c), three peaks appearing at 529.7, 531.2 and 532.5 eV were assigned to anhydrous manganese oxides (Mn–O–Mn), hydrated manganese oxides (Mn–O–H) and residual structure water (H–O–H), respectively.[34–36] The Mn–O–H peak located at 531.2 eV could be attributed to chemisorbed hydroxyl species at the MnO_2 surface, when exposed to ambient conditions. The high-resolution of C 1s spectrum (Fig. 4d) showed a main peak at 284.8 eV, which was corresponded to the binding energy of the sp^2 C–C bonds. The signal of the C 1s is from the RGO and CC. Based on these results, it can be concluded that CC/RGO/MnO_2 electrode has been successfully synthesized *via* this method.

To evaluate the structure design, the electrochemical properties of the CC/RGO and the CC/RGO/MnO_2 electrodes as supercapacitor electrodes were tested for comparison. Fig. 5a was CV curve for the CC/RGO and the CC/RGO/MnO_2 electrodes at a scan rate of 5 mV s^{-1} in the potential window of 0–0.8 V. The current values of CV for the CC/RGO/MnO_2 electrode were much higher than that of CC/RGO electrode at the same scan rate, therefore, the CC/RGO/MnO_2 electrode exhibits a higher area under the CV curve than CC/RGO electrode, which indicated the higher specific capacitance of CC/RGO/MnO_2 electrode. These results indicated that synergistic effects between RGO and MnO_2 cause a desirable capacitance enhancement. Fig. 5b showed the CV curves of the CC/RGO/MnO_2 electrode at different scan rates of 5, 10, 20, 50, and 100 mV s^{-1}, respectively. It can be seen that the CV curve can maintain a nearly rectangular shape at lower scan rates. However, the rectangular shape is distorted at scan rates over 50 mV s^{-1}. As one of typical carbon materials, RGO used as a supercapacitor electrode material provides double-layer capacitance. Compared with CC/RGO/MnO_2 electrode, the capacitance contributed by CC/RGO electrode is very small, which indicate that the high specific capacitance is mainly due to the pseudo-capacitance contribution of the MnO_2. However, no redox peaks are found in the CV curve, which is consistent with the electrochemical behavior of Mn-based electrode materials in neutral electrolytes. In this system, the main redox reaction equation is:[19,37]

$$MnO_2 + Na^+ + e^- \leftrightarrow MnOONa \quad (3)$$

However, no redox peaks were observed in our CV curves when the scan rates over 50 mV s^{-1}. This is mainly due to the charge storage process of the CC/RGO/MnO_2 electrode system is probably dominated by fast, reversible successive surface redox reactions.[38] Even more, ultrafine MnO_2 nanowires grew on the CC/RGO substrate which minimized the contact

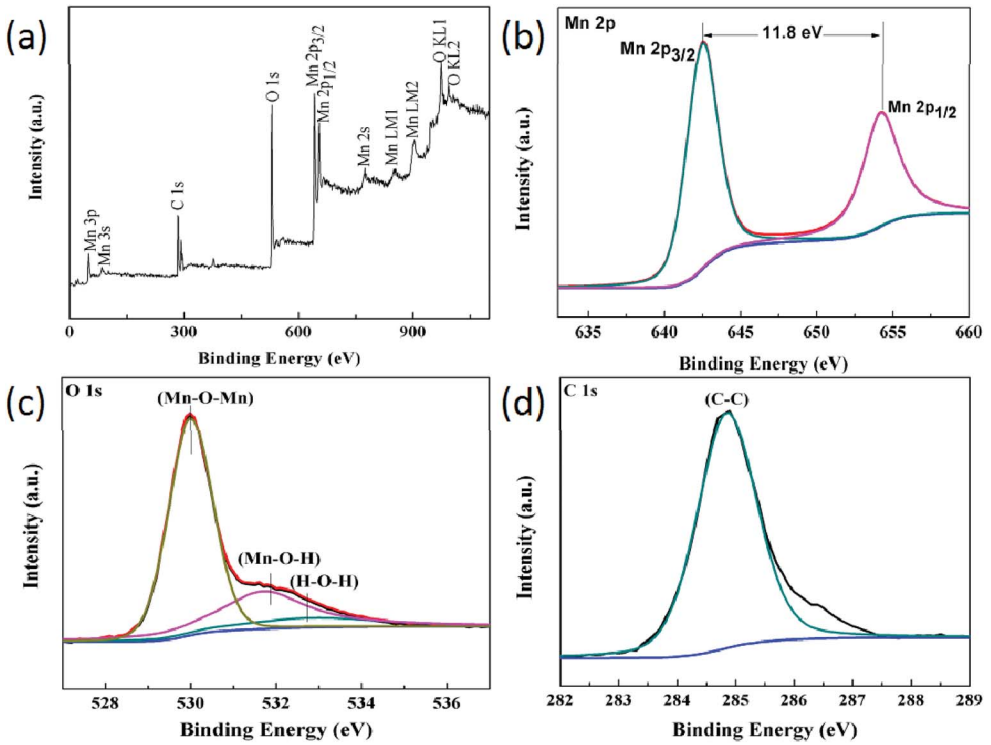

Fig. 4 (a) XPS survey of the CC/RGO/MnO_2. (b) Mn 2p XPS, (c) O 1s XPS and (d) C 1s XPS.

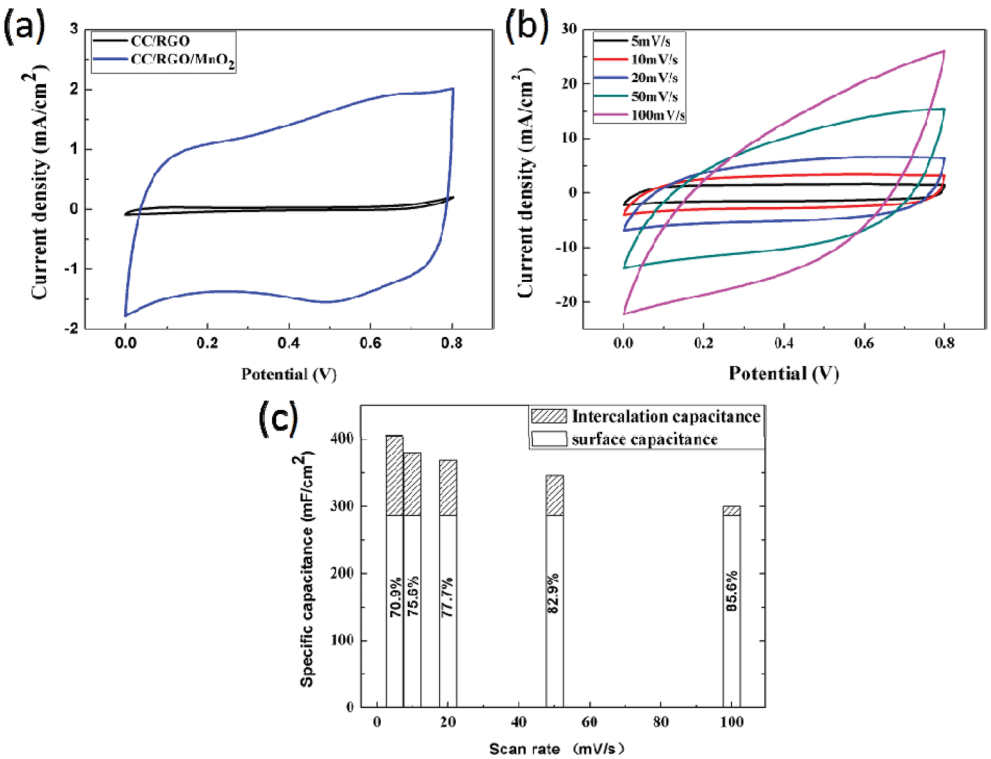

Fig. 5 (a) CV curves of the CC/RGO and the CC/RGO/MnO_2 electrodes at scan rate of 5 mV s^{-1}. (b) CV curves of the CC/RGO/MnO_2 electrode at different scan rates. (c) Comparison of storage for the CC/RGO/MnO_2 electrode nanocolumn arrays at scan rates of 5, 10, 20, 50, 100 mV s^{-1}, respectively.

resistance and allowed easier Faraday process of electrochemical active materials.

In fact, capacitive effects of electrode can be analyzed and discussed using the relationship between scan rate (v) and current (i):[39]

$$i = av^b \quad (4)$$

where a is the constant parameter, which depends on the nature of the electrode material, i is the current and v is the scan rate. The b-value is generally divided into two cases. If b-value is equal to 1.0, which i is proportional to v, capacitor contribution mainly comes from nondiffusion-controlled surface capacitive effects. On the other hand, if the b-value is equal to 0.5, which the inverse relationship between i and v, capacitance contribution mainly comes from the ideal diffusion-controlled intercalation process. Under normal circumstances, the charge storage of the electrode material is affected by both the surface capacitive and the diffusion control intercalation capacitance.

In addition, the charge storage contribution was calculated by following formula (5) and separated to be the percentages of surface capacitive effect and diffusion-controlled intercalation process.[40]

$$i(V) = k_1 v + k_2 v^{1/2} \quad (5)$$

The formula can be rearranged to

$$\frac{i(V)}{v^{1/2}} = k_1 v^{1/2} + k_2 \quad (6)$$

where $i(V)$ is electronic response current, v is scan rate, k_1 and k_2 are constants which are not affected by the scan rate. What's more, $k_1 v$ and $k_2 v^{1/2}$ correspond to the charge contributions from surface charge accumulation and diffusion-controlled intercalation, respectively.[41] At a certain voltage, we obtain an $i(V)/v^{1/2}$ and $v^{1/2}$ line under different $v^{1/2}$, where the slope is k_1 and the intercept with the Y axis is k_2. Fig. 5c describes the total areal capacitance, surface capacitance, and intercalation capacitance as a function of scan rate, which enables us to determine the fraction of surface capacitance from the total capacitance. It can be observed that the total capacitance decreased with the increase of scan rate. This phenomenon is attributed to the fact that intercalation process cannot keep up with the potential change at high scan rate.[42] The cause may be that there was insufficient time available for positive ions (H^+ and Na^+) to reach the inner small pores of the MnO_2 materials at high scan rate and hence they were mostly adsorbed on the outer surface of the electrode,[22,43] while at lower scan rate, cations could effectively diffuse into all the available spaces of electrode materials and thus lead to abundant insertion reaction to obtain a high specific capacitance.[44–47] Therefore, only the intercalation part decreases with the increase of scan rate, whereas the surface capacitance keeps almost constant.

In order to further find the charge storage capacity quantitatively, GCD measurements at different current densities are shown in Fig. 6a. Base on the discharge curves and the formula (1), the discharge-specific capacitances of the CC/RGO/MnO_2 electrode was calculated from the discharge curves to be 506.8 mF cm^{-2}, 474.8 mF cm^{-2}, 445.4 mF cm^{-2}, 419.8 mF cm^{-2}, 382.72 mF cm^{-2} at the current densities of 0.128, 0.256, 0.64, 1.28, 2.56 mA cm^{-2}, respectively. As the same time, the results present a trend that the specific capacitance gradually decreases with increasing of the current density (Fig. 6b), and it has a good rate capability of 75.5%. In addition, there is no obvious "IR" drop in the GCD curve, revealing excellent rate capacitive characteristics and reversible faradaic reaction between Na^+ and the ultrafine MnO_2 nanowires,[48] which is consistent with the CV results. In order to evaluate the flexibility of the CC/RGO/MnO_2 electrode, the electrode is bent 90° to be tested (marked the CC/RGO/MnO_2 (90)). Fig. 6c shows GCD curves for the CC/RGO/MnO_2 and the CC/RGO/MnO_2 (90) electrodes at the current density of the 0.128 mA cm^{-2}. As shown in the Fig. 6c, the shape of the GCD curves remained the same, indicating the retention of capacitive performance even in bent states. This result demonstrates the outstanding flexibility of the CC/RGO/MnO_2 electrode. Long cycle life is one of the key factors in the practical application of supercapacitors. Therefore, the electrochemical cyclic stability of the CC/RGO/MnO_2 electrodes is characterized by repeated charge and discharge tests at 1.28 mA cm^{-2} current density. The illustration in Fig. 6d was corresponding to charge–discharge curves of the first 2 and last 2 cycles of the CC/RGO/MnO_2 electrode. It can be seen that there are 98.6% of capacitance retention for the CC/RGO/MnO_2 electrode even after 10 000 cycles, which demonstrating the excellent cyclic stability of the CC/RGO/MnO_2 electrode. The reason for such excellent performance may be concluded as follows: synergistic effect in heterostructure, the intermediate RGO layer and the binder-free equipment method, thus improved the electrochemical performance.

Fig. 7a showed EIS spectra of the CC/RGO, CC/MnO_2 and CC/RGO/MnO_2 electrodes in a frequency range from 0.1 Hz to 100 kHz at open circuit voltage with the amplitude of 5 mV. The Nyquist curve is plotted with the real part (Z') as the abscissa and the imaginary part ($-Z''$) as the ordinate. The EIS spectrum of the CC/RGO, CC/MnO_2 and CC/RGO/MnO_2 electrodes present partial semicircles and a straight line with a higher slope. The EIS spectra of the CC/RGO electrode presents a larger diameter semicircle that confirms its high resistance. However, the EIS spectra of CC/MnO_2 and CC/RGO/MnO_2 electrodes contain a smaller diameter semicircle and a straight line with a larger slope, which confirm the high electronic and electron movement. Theoretically, RGO has better conductivity. However, due to the van der Waals' force between the graphene layers, it is easy to agglomerate between the molecular layers, which would introduce a new contact resistance to thermal transport in the graphene–graphene.[49] In our work, we use a solution dipping method to synthesize the CC/RGO. With the increase of graphene loading mass, graphene–graphene agglomerate result in the increase of resistance. In addition, the ultrafine structure of MnO_2 nanowires synthesized in this study promote the conductivity of the material. Hence, CC/MnO_2 exhibits a lower resistance than CC/GRO. The impedance spectra confirms that the hybrid can utilize the advantages of the MnO_2 and the RGO providing a faster highway for ion and

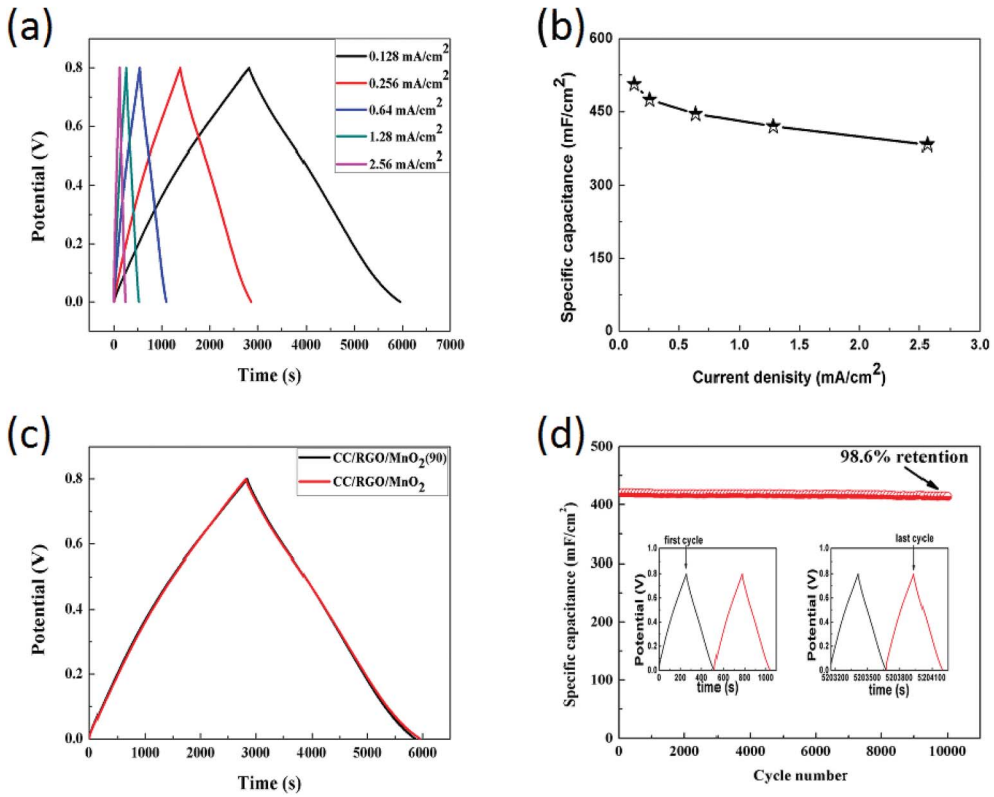

Fig. 6 (a) GCD curves of the CC/RGO/MnO_2 electrode under the different current densities. (b) Specific capacitances of the CC/RGO/MnO_2 electrode at different current density. (c) GCD curves of the CC/RGO/MnO_2 and the CC/RGO/MnO_2 (90) electrode at a current density of 0.128 mA cm^{-2}. (d) Cycling retention of the CC/RGO/MnO_2 electrode during galvanostatic cycling at 1.28 mA cm^{-2}.

electron movement. Therefore, it was confirmed that MnO_2 was designed on the conductive skeleton to improve its ion and electron conductivity to enhance its capacitance performance. The equivalent circuit diagram for fitting the EIS data was shown in the inset of Fig. 7a, consisting of the bulk solution resistance (R_s) in connection with a parallel circuit consisting of a charge-transfer resistance (R_{ct}) in series with a capacitor element (C_p) to account for the pseudo-capacitance and a constant phase element (CPE) to account for the double-layer capacitance.[50] In the high-frequency region (inset in Fig. 7a), we can see that the solution resistance of the CC/RGO/MnO_2 electrode is 3.03 Ω and the high frequency capacitance arc diameter shows that the charge transfer resistance is 5.5 Ω. In the middle-frequency region, the 45° sloped portion known as the Warburg resistance is the consequence of the frequency dependency of ion transport in the electrolyte, which suggesting that the electrochemical capacitive behavior of the CC/RGO/MnO_2 electrode is not controlled by diffusion,[51] which indicating that the CC/RGO/MnO_2 electrode exhibits good electrochemical performance. Furthermore, the slop of the line is observed to be higher than 45° in the low-frequency region, suggesting the predominance of pseudocapacitance.[52] In short,

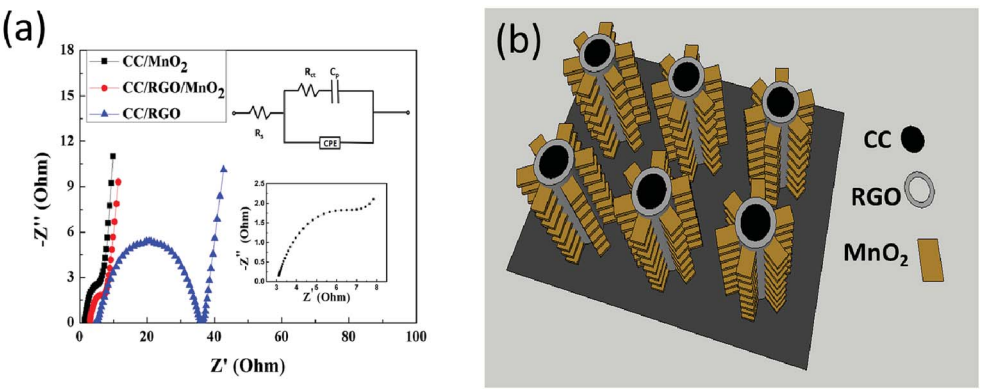

Fig. 7 (a) EIS spectra of the CC/RGO, CC/MnO_2 and CC/RGO/MnO_2 electrodes. (b) Schematic of the advantage in the charge storage of the as-prepared ultrafine MnO_2 nanowires@CC electrode.

the analysis of EIS indicates that the CC/RGO/MnO_2 electrode possesses an excellent capacitive performance, and this result agrees with the analysis of CV and GCD.

Compared with CC/RGO electrode, CC/RGO/MnO_2 electrode has much higher specific capacitance, and the electrochemical test results indicate that the CC/RGO/MnO_2 electrode can be regarded as being advantageous for electrochemical energy applications. This might be attributed to its unique architecture, as described in Fig. 7b. First, the interconnected 3D structure of the CC as skeleton can provides enough space for the electrolyte and avoids the aggregation of MnO_2 nanowires during ongoing charge/discharge processes. Besides, this skeleton can enlarge the electrode/electrolyte contact area, and provide more ion adsorption sites for double-layer formation and charge-transfer reactions. Second, after the CC is coated with the RGO layer, the CC/RGO as skeleton can provide large surface to volume. Furthermore, carbon is a good electrically conductive material and served as an electron transfer channel, which can provide fast electron transfer for faradic reactions. Third, each MnO_2 nanowire has its own electric contact with the substrate and thus can ensure all nanowires participate in the electrochemical reaction, which enhances the utilization of active materials. What's more, the MnO_2 nanowires loaded on the CC/RGO were quite fine, which promoted electrolyte diffusion into the inner region of the electrode, especially to reduce the internal resistance. In addition, 3D CC/RGO/MnO_2 electrode needs no binders or conducting additives, which decrease extra contact resistance or weight. In summary, the enhanced supercapacitor performances may be due to its unique structure providing fast ion and electron transfer, large reaction surface area and good electrochemical activity.

4. Conclusions

Through the simple "dipping method" and "hydrothermal method", CC/RGO/MnO_2 electrode with good flexibility is synthesized. The supercapacitor properties of CC/RGO/MnO_2 electrode were studied through electrochemical measurements and the results showed a high specific capacitance and long-life cyclic stability, due to the synergistic effect between the RGO and ultrafine MnO_2 nanowires. A maximum specific capacitance of 506.8 mF cm^{-2} was gained from the CC/RGO/MnO_2 electrode and electrochemical performance remains unchanged when the electrode is bent to 90°, displaying that the electrode has excellent flexibility. And it also showed good rate capability of 75.5% and high capacitance remained of 98.6%, which indicated that the CC/RGO/MnO_2 electrode could be used for high performance supercapacitor applications.

Conflicts of interest

There are no conflicts to declare.

Acknowledgements

This work was financially supported by the National Natural Science Foundation of China(11504267, 11504269), the Doctoral Fund of Tianjin Normal University (52XB1518) and Tianjin municipal education commission scientific research project (2017KJ238).

References

1 L. Li, K. Xia, L. Li, S. Shang, Q. Guo and G. Yan, Fabrication and characterization of free-standing polypyrrole/graphene oxide nanocomposite paper, *J. Nanopart. Res.*, 2012, **14**, 2–8.
2 X. Li and B. Wei, Supercapacitors based on nanostructured carbon, *Nano Energy*, 2013, **2**, 159–173.
3 A. Ramadoss and S. J. Kim, Improved activity of a graphene–TiO_2 hybrid electrode in an electrochemical supercapacitor, *Carbon*, 2013, **63**, 434–445.
4 I. S. I. Web, S. This, H. Press, N. York and A. Nw, Toward Flexible Batteries, *Science*, 2013, **319**, 737–738.
5 L. Nyholm, G. Nyström, A. Mihranyan and M. Strømme, Toward Flexible Polymer and Paper-Based Energy Storage Devices, *Adv. Mater.*, 2011, **23**, 3751–3769.
6 X. Lu and Y. Xia, Electronic materials: buckling down for flexible electronics, *Nat. Nanotechnol.*, 2006, **1**(3), 163–164.
7 W. Xu, S. Dai, G. Liu, Y. Xi, C. Hu and X. Wang, CuO Nanoflowers growing on Carbon Fiber Fabric for Flexible High-Performance Supercapacitors, *Electrochim. Acta*, 2016, **203**, 1–8.
8 X. Lu, M. Yu, G. Wang and Y. Tong, Flexible solid-state supercapacitors: design, fabrication and applications, *Energy Environ. Sci.*, 2014, **7**(7), 2160–2181.
9 X. Cai, M. Peng, X. Yu, Y. Fu and D. Zou, Flexible planar/fiber-architectured supercapacitors for wearable energy storage, *J. Mater. Chem. C*, 2014, **2**(7), 1184–1200.
10 X. Wang, X. Lu, B. Liu, D. Chen, Y. Tong and G. Shen, Flexible Energy-Storage Devices: Design Consideration and Recent Progress, *Adv. Mater.*, 2014, **26**(28), 4763–4782.
11 N. Yu, H. Yin, W. Zhang, Y. Liu, Z. Tang and M. Zhu, High-Performance Fiber-Shaped All-Solid-State Asymmetric Supercapacitors Based on Ultrathin MnO_2 Nanosheet/Carbon Fiber Cathodes for Wearable Electronics, *Adv. Energy Mater.*, 2016, **6**, 1–9.
12 Z. Ma, G. Shao, Y. Fan, G. Wang, J. Song and D. Shen, Construction of Hierarchical α-MnO_2 Nanowires@Ultrathin δ-MnO_2 Nanosheets Core–Shell Nanostructure with Excellent Cycling Stability for High-Power Asymmetric Supercapacitor Electrodes, *ACS Appl. Mater. Interfaces*, 2016, **8**, 9050–9058.
13 G. Han, Y. Liu, L. Zhang, E. Kan, S. Zhang, J. Tang and W. Tang, MnO_2 Nanorods Intercalating Graphene Oxide/Polyaniline Ternary Composites for Robust High-Performance Supercapacitors, *Sci. Rep.*, 2014, 1–7.
14 N. Zhang, Y. Ding, J. Zhang, B. Fu, X. Zhang and X. Zheng, Construction of MnO_2 nanowires@$Ni_{1-x}Co_xO_y$ nanoflake core–shell heterostructure for high performance supercapacitor, *J. Alloys Compd.*, 2017, **694**, 1302–1308.
15 W. Li, Q. Liu, Y. Sun, J. Sun, R. Zou, G. Li, X. Hu and G. Song, MnO_2 ultralong nanowires with better electrical conductivity and enhanced supercapacitor performances, *J. Mater. Chem.*, 2012, **22**, 14864–14867.

16 H. N. Jia, J. H. Lin, Y. L. Liu, S. L. Chen, Y. F. Cai, J. L. Qi, J. C. Feng and W. Fei, Nanosized core–shell structured graphene–MnO_2 nanosheet arrays as stable electrodes for superior supercapacitors, *J. Mater. Chem. A*, 2017, **5**, 10678–10686.

17 J. Balach, M. M. Bruno, N. G. Cotella, D. F. Acevedo and C. A. Barbero, Electrostatic self-assembly of hierarchical porous carbon microparticles, *J. Power Sources*, 2012, **199**, 386–394.

18 Y. Zhang, H. Feng, X. Wu, L. Wang, A. Zhang, T. Xia, H. Dong, X. Li and L. Zhang, Progress of electrochemical capacitor electrode materials: A review, *Int. J. Hydrogen Energy*, 2009, **34**, 4889–4899.

19 S. Yang, P. Yan, Y. Li, K. Cheng, K. Ye, C. Zhang and D. Cao, Reduced graphene oxide decorated on MnO_2 nanoflakes grown on C/TiO_2 nanowire arrays for electrochemical energy storage, *RSC Adv.*, 2015, **5**, 87521–87527.

20 H. Chou, A. Nguyen, A. Chortos, J. W. F. To, C. Lu, J. Mei, T. Kurosawa, W. Bae, J. B. Tok and Z. Bao, A chameleon-inspired stretchable electronic skin with interactive colour changing controlled by tactile sensing, *Nat. Commun.*, 2015, **6**, 1–10.

21 Y. M. Dai, S. C. Tang, J. Q. Peng, H. Y. Chen, Z. X. Ba, Y. J. Ma and X. K. Meng, MnO_2@SnO_2 core–shell heterostructured nanorods for supercapacitors, *Mater. Lett.*, 2014, **130**, 107–110.

22 Z. Xu, S. Sun, W. Cui, J. Lv, Y. Geng, H. Li and J. Deng, Interconnected network of ultrafine MnO_2 nanowires on carbon cloth with weed-like morphology for high-performance supercapacitor electrodes, *Electrochim. Acta*, 2018, **268**, 340–346.

23 J. Hu, F. Qian, G. Song, W. Li and L. Wang, Ultrafine MnO_2 Nanowire Arrays Grown on Carbon Fibers for High-Performance Supercapacitors, *Nanoscale Res. Lett.*, 2016, **11**, 2–7.

24 R. Hu, J. Zhao, R. Jiang and J. Zheng, Preparation of high strain Polyaniline/polyvinyl alcohol composite and its applications in stretchable supercapacitor, *J. Mater. Sci.: Mater. Electron.*, 2017, **28**, 14568–14574.

25 S. Murali, M. D. Stoller, C. Morales, A. Velamakanni, Y. W. Zhu and R. Ruoff, Ultracapacitor performance of reduced graphene oxide-silica composite, in *Electrochemistry of Novel Materials for Energy Storage and Conversion*, ECS Meeting, 2011, vol. 99–104.

26 J. Xia, F. Chen, J. Li and N. Tao, Measurement of the quantum capacitance of graphene, *Nat. Nanotechnol.*, 2009, **4**, 505–509.

27 S. R. C. Vivekchand, C. S. Rout, K. S. Subrahmanyam, A. Govindaraj and C. N. R. Rao, Graphene-based electrochemical supercapacitors, *J. Chem. Sci.*, 2008, **120**, 9–13.

28 P. Yu, Y. Li, X. Zhao, L. Wu and Q. Zhang, Graphene-wrapped polyaniline nanowire arrays on nitrogen-doped carbon fabric as novel flexible hybrid electrode materials for high-performance supercapacitor, *Langmuir*, 2014, **30**, 5306–5313.

29 B. Yao, L. Huang, J. Zhang, X. Gao, J. Wu, Y. Cheng, X. Xiao, B. Wang, Y. Li and J. Zhou, Flexible Transparent Molybdenum Trioxide Nanopaper for Energy Storage, *Adv. Mater.*, 2016, 6353–6358.

30 B. Wang, J. Qiu, H. Feng, N. Wang, E. Sakai and T. Komiyama, Preparation of MnO_2/carbon nanowires composites for supercapacitors, *Electrochim. Acta*, 2016, **212**, 710–721.

31 J. Zhang, Y. Wang and J. Zang, Electrophoretic deposition of MnO_2 -coated carbon nanotubes on a graphite sheet as a flexible electrode for supercapacitors, *Carbon*, 2012, **50**, 5196–5202.

32 C. Yang, M. Zhou and Q. Xu, Three-dimensional ordered macroporous MnO_2/carbon nanocomposites as high-performance electrodes for asymmetric supercapacitors, *Phys. Chem. Chem. Phys.*, 2013, **15**, 19730.

33 H. Wang, Z. Lu, D. Qian, Y. Li and W. Zhang, Single-crystal α-MnO_2 nanorods: Synthesis and electrochemical properties, *Nanotechnology*, 2007, **18**, 1–5.

34 T. Cottineau, M. Toupin, T. Delahaye, T. Brousse and D. Bélanger, Nanostructured transition metal oxides for aqueous hybrid electrochemical supercapacitors, *Appl. Phys. A: Mater. Sci. Process.*, 2006, **82**, 599–606.

35 V. H. Nguyen, V. C. Tran, D. Kharismadewi and J. Shim, Ultralong MnO_2 nanowires intercalated graphene/Co_3O_4 composites for asymmetric supercapacitors, *Mater. Lett.*, 2015, **147**, 123–127.

36 V. H. Nguyen and J. Shim, The 3D Co_3O_4/graphene/nickel foam electrode with enhanced electrochemical performance for supercapacitors, *Mater. Lett.*, 2015, **139**, 377–381.

37 S. Yang, K. Cheng, J. Huang, K. Ye, Y. Xu, D. Cao, X. Zhang and G. Wang, High-capacitance MnO_2 nanoflakes on preformed C/TiO_2 shell/core nanowire arrays for electrochemical energy storage, *Electrochim. Acta*, 2014, **120**, 416–422.

38 P. Simon and Y. Gogotsi, Materials for electrochemical capacitors, *Nat. Mater.*, 2008, **7**, 845–854.

39 R. Wang, C. Xu and J. M. Lee, High performance asymmetric supercapacitors: new NiOOH nanosheet/graphene hydrogels and pure graphene hydrogels, *Nano Energy*, 2016, **19**, 210–221.

40 C. Tanggarnjanavalukul, N. Phattharasupakun, K. Kongpatpanich and M. Sawangphruk, Charge storage performances and mechanisms of MnO_2 nanospheres, nanorods, nanotubes and nanosheets, *Nanoscale*, 2017, **9**(36), 13630.

41 H. Yin, C. Song, Y. Wang, S. Li and M. Zeng, Influence of morphologies and pseudocapacitive contributions for charge storage in V_2O_5, micro/nano-structures, *Electrochim. Acta*, 2013, **111**(6), 762–770.

42 Y. Yuan, W. Wang, J. Yang and H. Tang, Three-dimensional $NiCo_2O_4$@$MnMoO_4$ core–shell nanoarrays for high-performance asymmetric supercapacitors, *Langmuir*, 2017, **33**, 40.

43 D. Yu and L. Dai, Self-Assembled Graphene/Carbon Nanotube Hybrid Films for Supercapacitors, *J. Phys. Chem. C*, 2010, **1**, 467–470.

44 J. Zhu and J. He, Facile Synthesis of Graphene-Wrapped Honeycomb MnO2 Nanospheres and Their Application in Supercapacitors, *ACS Appl. Mater. Interfaces*, 2012, **4**, 1770–1776.

45 S. Ren, Y. Yang, M. Xu, H. Cai, C. Hao and X. Wang, Physicochemical and Engineering Aspects Hollow SnO2 microspheres and their carbon-coated composites for supercapacitors, *Colloids Surf., A*, 2014, **444**, 26–32.

46 Z. J. Li, T. X. Chang, G. Q. Yun and Y. Jia, Coating single walled carbon nanotube with SnO_2 and its electrochemical properties, *Powder Technol.*, 2012, **224**, 306–310.

47 Z. Luo, E. Liu, T. Hu, Z. Li, T. Liu and L. Song, *Synthesis of polyaniline/SnO_2 nanocomposite and its improved electrochemical performance*, Elsevier Ltd, 2014, vol. 60, pp. 105–110.

48 S. Liao, K. Holmes, H. Tsaprailis and V. I. Birss, High performance PtRuIr catalysts supported on carbon nanotubes for the anodic oxidation of methanol, *J. Am. Chem. Soc.*, 2006, **128**, 3504–3505.

49 Y. Su, J. J. Li and G. J. Weng, Theory of thermal conductivity of graphene-polymer nanocomposites with interfacial Kapitza resistance and graphene-graphene contact resistance, *Carbon*, 2018, **137**, 222–233.

50 M. Toupin, T. Brousse and D. Bélanger, Charge storage mechanism of MnO_2 electrode used in aqueous electrochemical capacitor, *Chem. Mater.*, 2004, **16**, 3184–3190.

51 Y. Zhang, Z. Hu, Y. Liang, Y. Yang, N. An, Z. Li and H. Wu, Growth of 3D SnO_2 nanosheets on carbon cloth as a binder-free electrode for supercapacitors, *J. Mater. Chem. A*, 2015, **3**, 15057–15067.

52 X. Jian, S. Liu, Y. Gao, W. Zhang, W. He, A. Mahmood, C. M. Subramaniyam, X. Wang, N. Mahmood and S. X. Dou, Facile Synthesis of Three-Dimensional Sandwiched MnO_2@GCs@MnO_2 Hybrid Nanostructured Electrode for Electrochemical Capacitors, *ACS Appl. Mater. Interfaces*, 2017, **9**, 18872–18882.